communications physics

ARTICLE

https://doi.org/10.1038/s42005-021-00700-6 OPEN

Fundamental limits and optimal estimation of the resonance frequency of a linear harmonic oscillator

Mingkang Wang [1,2], Rui Zhang[3], Robert Ilic [1], Yuxiang Liu[3] & Vladimir A. Aksyuk [1✉]

All physical oscillators are subject to thermodynamic and quantum perturbations, fundamentally limiting measurement of their resonance frequency. Analyses assuming specific ways of estimating frequency can underestimate the available precision and overlook unconventional measurement regimes. Here we derive a general, estimation-method-independent Cramer Rao lower bound for a linear harmonic oscillator resonance frequency measurement uncertainty, seamlessly accounting for the quantum, thermodynamic and instrumental limitations, including Fisher information from quantum backaction- and thermodynamically driven fluctuations. We provide a universal and practical maximum-likelihood frequency estimator reaching the predicted limits in all regimes, and experimentally validate it on a thermodynamically limited nanomechanical oscillator. Low relative frequency uncertainty is obtained for both very high bandwidth measurements ($\approx 10^{-5}$ for $\tau = 30\,\mu s$) and measurements using thermal fluctuations alone ($<10^{-6}$). Beyond nanomechanics, these results advance frequency-based metrology across physical domains.

[1] Microsystems and Nanotechnology Division, National Institute of Standards and Technology, Gaithersburg, MD, USA. [2] Institute for Research in Electronics and Applied Physics, University of Maryland, College Park, MD, USA. [3] Department of Mechanical Engineering, Worcester Polytechnic Institute, Worcester, MA, USA. ✉email: vladimir.aksyuk@nist.gov

Parametrically coupling time-varying unknown quantities to resonance frequencies of harmonic oscillators enables measurements that are insensitive to low-frequency noise sources and drifts in the detection gain and bias. The unmatched performance of frequency-based sensing makes it the core of accurate scientific and cost-effective commercial measurement systems, spanning the length scales from kilometer-long LIGO[1] to mesoscopic micro- and nano-electro-mechanical systems (M/NEMs)[2–9] and further to the single-atom tip of a frequency-modulation atomic force microscope (AFM)[10].

Despite the wide applications of frequency-based sensing for scientific high-precision measurement, a general and fundamental understanding of the linear oscillator resonance frequency estimation and its uncertainty limits is currently lacking. The thermodynamic limit for frequency measurement has been considered separately in the AFM community[11] and M/NEMs community[12,13]. However, due to specific assumptions and simplifications regarding measurement conditions and how the frequency is calculated from the position data, the reported thermodynamic limits are different from each other and only valid for specific measurement regimes[12–16], such as for strongly driven oscillators with negligible detection noise in the long averaging time limit. Additionally, the thermodynamic fluctuations of the oscillator motion, typically only considered as a source of uncertainty, in fact also contain information about the resonance frequency, evident, for example, from the Lorentzian peak in its thermal noise power spectral density. Yet this additional frequency information is not only missed in many frequency measurement settings, but also overlooked when analyzing the fundamental measurement limits, radically underestimating the available precision for frequency estimation in situations where the magnitude of the available external driving force is limited.

Information theory provides a Cramer Rao lower bound (CRLB)[17–19] for the uncertainty of unbiased parameter estimation from a set of measured data, valid regardless of any specific estimation procedure. The bound uses the total Fisher information[20] about the unknown parameter obtained by the measurement, relying only on the underlying relationship between the parameter and the data, namely the conditional probability of obtaining the particular measured data for the specific value of the parameter. Due to its universality, it has been widely applied to obtain measurement limits and benchmark specific measurements, such as super-resolution ultrasonic[21] and optical microscopy[22], particle tracking and localization[23,24], and the standard quantum limit for entangled or squeezed states[25,26].

Here, we derive the CRLB to obtain general uncertainty limits, including the fundamental quantum and thermodynamic limits, as well as the instrumental limits, for resonance frequency extracted from continuous position measurement of a linear harmonic oscillator (LHO), subject to dissipation, thermodynamic- and quantum-backaction-induced stochastic fluctuations, instrumental detection uncertainty, and external harmonic excitation. Acknowledging that a nondemolition frequency detection is ideal in the quantum regime, we remain focused on the continuous measurement of position, encountered in most experimental situations. In addition to recovering the uncertainty minimum of the standard quantum limit expected for such measurement under strong coherent external excitation, we present the fundamental limits of extracting the frequency information from fluctuations driven by the quantum measurement itself solely, or in combination with thermal and external driving forces. Besides, we propose a computationally fast and statistically efficient frequency estimator—a procedure for converting the detected motion into the frequency in real-time with imprecision not exceeding their theoretical limits given by the CRLB. The proposed estimator extracts the frequency information simultaneously from the harmonic response and the stochastic fluctuations, while optimally averaging over the detection noise, making it applicable on all time scales and with any external driving strength. Far beyond the conventionally used phase[14] and Kay's (phase gradient)[27] estimators, it can be directly applied to data of low signal-to-noise-ratio(SNR) extracting all available frequency information. Based on our knowledge, the derived frequency detection limit and estimator cover all specific conditions considered in previous works.

Using the proposed frequency estimator, we experimentally measure resonance frequency of a low-loss stress-engineered thermodynamically limited nanomechanical resonator with integrated photonic cavity-optomechanical readout. We demonstrate the frequency uncertainty (Allan deviation[28]) reaching the theoretical lower limit (CRLB) over 4 decades of measurement bandwidth (averaging time τ) with a relative precision of $\approx 0.4 \times 10^{-6}$ for frequency measured without excitation, using only thermodynamic fluctuations at room temperature, which is better than the average performance of state-of-the-art NEMs under strong driving force in this mass range (≈1 pg)[15]. Distinct from exploiting the full driven linear dynamic range of our device, here we focus on quantitatively understanding the uncertainty limits and making the best possible measurement with a given driving force. The measurement in the limit of weak or no driving force works surprisingly well for nanoscale systems at room temperature and may extend to other domains and to quantum backaction-driven measurements.

Results

Oscillator motion in a rotating frame and the experimental system. As shown in Fig. 1(a), we consider a LHO subject to dissipation Γ, white fluctuating force f, which includes a Langevin force coming from a thermal bath and a quantum measurement backaction force. An harmonic driving force $F = F_0\cos(\omega t)$ with a magnitude F_0 at frequency ω may also be applied. The equation of motion for the classical LHO is written as:

$$\ddot{x} + \Gamma\dot{x} + \omega_0^2 x = \frac{F(t) + f}{m} \tag{1}$$

where x is the position of the LHO, m is the effective mass, and ω_0 is its resonance frequency. The fluctuating force is assumed to be frequency independent, at least over the resonator bandwidth, and therefore effectively obeying $\langle f(t)f(t')\rangle = f_{rms}^2\delta(t-t')$ with a constant f_{rms}^2. Specifically, for thermodynamic fluctuations $f_{rms}^2 = 2\Gamma k_b T m$ based on the fluctuation-dissipation theorem, k_b is the Boltzmann constant, T is the effective temperature, while for quantum backaction $f_{rms}^2 = 2k\hbar^2$ for position measurement strength k [Supplementary Note 8: Eq. (S74)].

The LHO undergoes a continuous position measurement, recorded by a detector with a detection uncertainty. The position trace is fed into a frequency estimator to obtain an estimated eigenfrequency $\hat{\omega}_0$. The frequency uncertainty $\sigma_f(\tau)$ is a function of averaging time τ and depends on the driving force, the stochastic fluctuating forces, and the detection uncertainty. When the LHO is used for sensing, the eigenfrequency varies in time due to the parametric interaction between the LHO and the measured quantities. For a fixed interaction strength, the uncertainty of the estimated eigenfrequency directly translates to the uncertainty of the measured quantities, limiting the measurement precision.

The LHO used in the experiment is a nano-scale tuning fork made from high tensile stress silicon nitride [false-colored

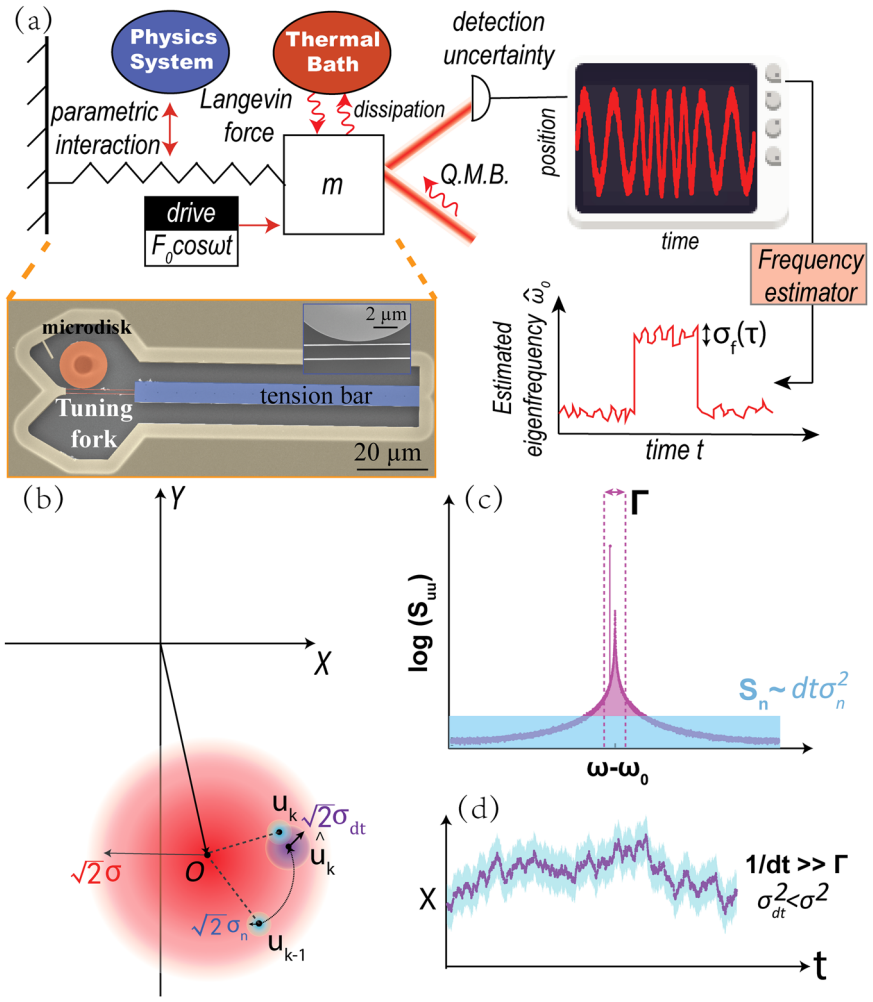

Fig. 1 Measurement of resonance frequency. a A linear harmonic oscillator subject to a driving force, stochastic Langevin and quantum measurement backaction forces (QMB), and detection uncertainty. The time-varying eigenfrequency induced by a parametric interaction with an external system is extracted from the continuously measured position x [Eq.(1)] by a frequency estimator. Lower panel shows the false-colored scanning electron micrograph of the nanomechanical tuning fork with a cavity-optomechanical readout. Inset: a magnified view of the coupling gap between them. **b** The red bubble in the phase diagram represents the steady-state distribution of the linear harmonic oscillator (LHO) rotating-frame coordinate $u = X + iY$ [Eq. (2)] subject to thermal and quantum fluctuations. The purple bubble represents the distribution of u_k due to diffusion around the expectation $\hat{u}_k$, in a short time dt after a known state u_{k-1}. The blue bubbles show the position detection uncertainty. The red, purple, and blue distributions have a standard deviation of $\sqrt{2}\sigma$, $\sqrt{2}\sigma_{dt}$, and $\sqrt{2}\sigma_n$, respectively, in each of the two dimensions. The distance $\hat{u}_k - u_{k-1}$ is exaggerated for illustration. **c** LHO position power spectral density S_{uu}, when driven at a small detuning from a constant resonance frequency. The purple area denotes the contribution from the mechanical motion. The blue area represents the detection noise spectrum. **d** Real component X of u. Blue and purple dots schematically represent the measured positions with the detection uncertainty and actual positions without detection uncertainty, respectively.

micrograph in Fig. 1(a)]. The nominal thickness, width, and length of the tuning fork are 250 nm, 150 nm, and 20 μm, respectively. The tuning fork is stretched by a tension bar on the right-hand side to provide extra tensile stress. The highly enhanced tensile stress leads to a high frequency-Quality factor product of order 10^{12}. Due to the fluctuation-dissipation theorem, low damping leads to a smaller Langevin force, reducing the thermodynamically limited frequency measurement uncertainty, as derived below. The high resonance frequency serves to reduce the relative uncertainty of the measurement further. An electrostatic driving force is applied to the tuning fork from a sharp metal probe positioned in proximity to the fork. The mechanical motion of the tuning fork is measured through a near-field cavity-optomechanical readout (See Supplementary Note 1)[29] with detection noise well below the thermal fluctuation within the fork resonance linewidth.

By defining a slowly varying variable u via $x = \frac{1}{2}(ue^{i\omega t} + u^* e^{-i\omega t})$, we use the rotating wave approximation (RWA):

$$\dot{u} + \frac{\Gamma}{2}u - i\Delta\omega u = \frac{F_0}{2i\omega m} - \frac{f_1 - if_2}{i\omega m} \quad (2)$$

where $\Delta\omega = (\omega_0 - \omega) \ll \omega_0$ and $f_{1,2}$ are the in-phase and quadrature components of the fluctuation force in the rotating frame near resonance with $\langle f_i(t) f_j(t')\rangle = \frac{1}{2} f_{rms}^2 \delta(t - t')\delta_{ij}$. Note, the choice of the sign of Δω reflects that the accurately known driving/reference frequency ω is stable, while the resonance frequency ω_0 is the variable to be determined from the measurement.

In a steady state, u obeys a two-dimensional Gaussian distribution around the harmonic response $O(\Delta\omega) = \langle u\rangle = \frac{A\Gamma}{2\Delta\omega + i\Gamma}$, where $A = \frac{F_0}{m\omega_0\Gamma}$ [red bubble in Fig. 1(b)]. Defining fluctuating-force-induced variance of x around the harmonic response $x_{harmonic} =$

$|O|\cos(\omega t+\angle O)$ as $\sigma^2=\langle(x-x_{harmonic})^2\rangle$ and using $\langle x^2\rangle=\frac{1}{2}\langle|u|^2\rangle$ we obtain $\langle|u-O|^2\rangle=2\sigma^2$ [see Supplementary Note 2], i.e., u has a variance σ^2 for both in-phase, X, and quadrature, Y, components. For thermodynamic fluctuations, this variance $\sigma^2=\frac{k_bT}{m\omega_0{}^2}$ is given by the equipartition theorem, while generally:

$$\sigma^2=\frac{f_{rms}^2}{2\Gamma m^2\omega_0{}^2} \tag{3}$$

Consider a continuous position measurement of a series u_k at equal intervals $t_k=k\mathrm{d}t$ with $\mathrm{d}t\ll 1/\Gamma$. As shown in the phase diagram of Fig. 1(b), the LHO rotates around O at the rate $\Delta\omega$ and decays at the rate $\frac{\Gamma}{2}$, following Eq. (2), evolving deterministically from a known position u_{k-1} to an expected position $\hat{u}_k=O+(u_{k-1}-O)e^{\left(i\Delta\omega-\frac{\Gamma}{2}\right)\mathrm{d}t}$ in time $\mathrm{d}t$. Meanwhile, it also diffuses in response to the fluctuating force, arriving at the next actual position u_k. In the Markov diffusion process u_k depends only on u_{k-1}, and is independent of the prior history. Given a known value of u_{k-1}, for $\mathrm{d}t\ll 1/\Gamma$, the probability density $P\left(u_k|u_{k-1}\right)$ for u_k in the phase diagram is a 2-dimensional Gaussian [purple bubble in Fig. 1(b)] with a mean (expectation) value of $\hat{u}_k$ accounting for the deterministic evolution and variance of $\sigma_{\mathrm{d}t}^2$ for each dimension due to the random diffusion:

$$P(u_k|u_{k-1})=\frac{1}{2\pi\sigma_{\mathrm{d}t}^2}e^{-\frac{\left|(u_k-O)-(u_{k-1}-O)e^{\left(i\Delta\omega-\frac{\Gamma}{2}\right)\mathrm{d}t}\right|^2}{2\sigma_{\mathrm{d}t}^2}} \tag{4}$$

For $\mathrm{d}t\ll 1/\Gamma$, variance $\sigma_{\mathrm{d}t}^2\propto\mathrm{d}t$ can be quantitatively related to σ^2 by noting that the decay and diffusion balance each other in a steady state, resulting in [See Supplementary Note 2]:

$$\sigma_{\mathrm{d}t}^2=\Gamma\mathrm{d}t\sigma^2 \tag{5}$$

For illustration, we unphysically exaggerate the evolution of $\hat{u}_k$ in Fig. 1(b). In the continuous measurement limit ($\mathrm{d}t\ll 1/\Gamma$), the deterministic motion is always smaller than the stochastic one: $\hat{u}_k-u_{k-1}\ll\sqrt{2}\sigma_{\mathrm{d}t}$ as $(u_{k-1}-O)(i\Delta\omega-\frac{\Gamma}{2})\mathrm{d}t\ll\sigma\sqrt{2\Gamma\mathrm{d}t}$.

Figure 1(c) shows the power spectral density S_{uu} of the driven LHO with a small detuning $\Delta\omega$. The purple and blue areas display the mechanical noise and detection noise density, S_n. The blue (purple) dots in Fig. 1(d) shows the corresponding in-phase component of u, i.e., real part of u, in the time domain with (without) detection noise. The points separated by times $t\ll 1/\Gamma$ are correlated.

Cramer Rao Lower Bound and the detection uncertainty. To describe a position measurement with detection noise, we introduce u_{m}^k, an independent unbiased measurement of the actual position u_k. We now consider a finite time series $U_{\mathrm{m}}^N=\{u_{\mathrm{m}}^1,...u_{\mathrm{m}}^k...,u_{\mathrm{m}}^N\}$ of N complex values u_{m}^k measured over the time $\tau=(N-1)\mathrm{d}t$, and answer the question: how well the resonance frequency can in principle be estimated from such a measurement? With the RWA reference frequency ω perfectly known, the variance of the estimate $\hat{\omega}_0$ of an unknown resonance frequency ω_0 is equal to the variance of the estimated relative frequency $\widehat{\Delta\omega}=\hat{\omega}_0-\omega$. Note, the hat-marks denote the measured value. The theoretical lower bound on this variance is given by the CRLB[18]:

$$\mathrm{Var}(\widehat{\omega}_0)=\mathrm{Var}(\widehat{\Delta\omega})\geq\mathrm{I}(\Delta\omega)^{-1}=-\left[\left\langle\frac{\partial^2}{\partial\Delta\omega^2}\ln\mathrm{P}(U_{\mathrm{m}}^N,\Delta\omega)\right\rangle\right]^{-1} \tag{6}$$

where the quantity $\mathrm{I}(\Delta\omega)=-\left\langle\frac{\partial^2}{\partial\Delta\omega^2}\ln\mathrm{P}(U_{\mathrm{m}}^N,\Delta\omega)\right\rangle$ is the Fisher information, and $\mathrm{P}\left(U_{\mathrm{m}}^N,\Delta\omega\right)$ is a $2N$ dimensional probability density of obtaining a specific measurement U_{m}^N, with $\langle\ldots\rangle$ denoting the expectation for a given $\Delta\omega$.

For the white detection noise,

$$P(u_{\mathrm{m}}^k|u_k)=\frac{1}{2\pi\sigma_{\mathrm{n}}^2}e^{-\frac{\left|u_{\mathrm{m}}^k-u_k\right|^2}{2\sigma_{\mathrm{n}}^2}} \tag{7}$$

Similar to $\sigma_{\mathrm{d}t}^2$ and σ^2, $\sigma_{\mathrm{n}}^2=\langle(x_{\mathrm{m}}-x)^2\rangle\propto 1/\mathrm{d}t$ is the white-noise variance in each of the components of the 2-dimensional Gaussian in the RWA. Here we introduce a dimensionless parameter $\eta=\sqrt{\frac{\sigma_{\mathrm{n}}^2\Gamma\mathrm{d}t}{\sigma^2}}$ that is the ratio of the detection noise within the LHO bandwidth Γ and the stochastic position fluctuations due to the fluctuating forces.

Cramer Rao Lower Bound for frequency measurement of linear harmonic oscillators subject to detection noise

General classical CRLB for frequency measurement. White detection noise $\sigma_{\mathrm{n}}^2\propto 1/\mathrm{d}t$ will always exceed diffusion $\sigma_{\mathrm{d}t}^2=\Gamma\mathrm{d}t\sigma^2$ for a sufficiently small $\mathrm{d}t$, such as, for example, in a high bandwidth measurement of motion and resonance frequency. Explicitly accounting for the detection noise also allows us to directly extend the present classical analysis to a quantum LHO under a continuous quantum position measurement since it is mathematically equivalent to a classical LHO subject to specific levels of the detection uncertainty and the stochastic quantum backaction force[30,31].

In the classical case, while the transition from u_{k-1} to u_k is a Markov process, this is not so between the sequentially measured values u_{m}^k with detection noise. Each new measured value u_{m}^k generally depends on the previous history of measurements U_{m}^{k-1}. The probability of $\mathrm{P}\left(U_{\mathrm{m}}^N,\Delta\omega\right)$ must be derived using the underlying actual motion trajectory $U=\left\{u_1...,u_k,...u_N\right\}$ governed by Eq. (4), and the dependence of the measured value u_{m}^k on the actual position u_k via Eq. (7). The probability of obtaining the k-th measurement u_{m}^k after U_{m}^{k-1} depends on the conditional probability distribution of true position u_k, given previous measurements U_{m}^{k-1}.

$$\begin{aligned}\mathrm{P}\left(u_{\mathrm{m}}^k|U_{\mathrm{m}}^{k-1}\right)&=\int\mathrm{P}\left(u_{\mathrm{m}}^k|u_k\right)\mathrm{P}\left(u_k|U_{\mathrm{m}}^{k-1}\right)du_k\\&=\int\mathrm{P}\left(u_{\mathrm{m}}^k|u_k\right)\int\mathrm{P}\left(u_k|u_{k-1}\right)\mathrm{P}\left(u_{k-1}|U_{\mathrm{m}}^{k-1}\right)du_{k-1}du_k\end{aligned} \tag{8}$$

Here the likelihood $\mathrm{P}\left(u_{k-1}|U_{\mathrm{m}}^{k-1}\right)$ expresses the knowledge of the actual position u_{k-1} of LHO after a specific series of recorded measurements $U_{\mathrm{m}}^{k-1}=\left\{u_{\mathrm{m}}^1,...u_{\mathrm{m}}^{k-1}\right\}$. It can be computed via the recursive Bayesian update[32]:

$$\begin{aligned}\mathrm{P}\left(u_k|U_{\mathrm{m}}^k\right)&=\mathrm{P}\left(u_k|u_{\mathrm{m}}^k,U_{\mathrm{m}}^{k-1}\right)\propto\mathrm{P}\left(u_{\mathrm{m}}^k|u_k\right)\mathrm{P}\left(u_k|U_{\mathrm{m}}^{k-1}\right)\\&=P\left(u_{\mathrm{m}}^k|u_k\right)\int\mathrm{P}\left(u_k|u_{k-1}\right)\mathrm{P}\left(u_{k-1}|U_{\mathrm{m}}^{k-1}\right)du_{k-1}\end{aligned} \tag{9}$$

Starting with $\mathrm{P}(u_1)=\frac{1}{2\pi\sigma^2}e^{-\frac{\left|u_1-\widetilde{O(\Delta\omega)}\right|^2}{2\sigma^2}}$ with $\widetilde{O}=\frac{A\Gamma}{2\Delta\omega+i\Gamma}$ being a function of the resonance frequency $\widetilde{\Delta\omega}$ prior to the start of the measurement, $\mathrm{P}\left(u_k|U_{\mathrm{m}}^k\right)$ defines the knowledge of the LHO state during the measurement. Since all the functions in Eq. (9) are Gaussian, their products and integrals are Gaussian as well. For each time step k, the likelihood is a Gaussian with a mean value $\bar{u}_k$ and a standard deviation σ_k, defined by:

$$P(u_k|U_{\mathrm{m}}^k)=\frac{1}{2\pi\sigma_k^2}e^{-\frac{\left|(u_k-O)-\xi_k\right|^2}{2\sigma_k^2}} \tag{10}$$

where $\xi_k = \bar{u}_k - O(\Delta\omega)$ shifts the origin to $O(\Delta\omega)$, with the $\xi_0 = 0$ and $\sigma_0 = \sigma$ prior to any measurement.

Utilizing Eqs. (4), (7) and (10), the Bayesian update Eq. (9) can be expressed as an update $\xi_0 = 0$, $\sigma_0 = \sigma$, $\xi_{k-1} \to \xi_k$, $\sigma_{k-1} \to \sigma_k$ [Supplementary Note 6: A]:

$$\xi_k = \left[\frac{1}{(1-\Gamma dt)\sigma_{k-1}^2 + \sigma_{dt}^2} e^{\left(i\Delta\omega - \frac{\Gamma}{2}\right)dt}\xi_{k-1} + \frac{1}{\sigma_n^2}(u_m^k - O)\right] \times \left(\frac{1}{(1-\Gamma dt)\sigma_{k-1}^2 + \sigma_{dt}^2} + \frac{1}{\sigma_n^2}\right)^{-1} \tag{11}$$

$$\frac{1}{\sigma_k^2} = \frac{1}{(1-\Gamma dt)\sigma_{k-1}^2 + \sigma_{dt}^2} + \frac{1}{\sigma_n^2} \tag{12}$$

This update can be intuitively understood in two steps. First, the prior position is evolved in time dt via rotation and decay, $\xi_{k-1} \to e^{\left(i\Delta\omega - \frac{\Gamma}{2}\right)dt}\xi_{k-1}$, while the variance is decreased by the decay and increased by the diffusion $\sigma_{k-1}^2 \to \sigma_{k-1}^2 e^{-\Gamma dt} + \sigma_{dt}^2 = (1-\Gamma dt)\sigma_{k-1}^2 + \sigma_{dt}^2$ in the continuous measurement limit ($\Gamma dt \ll 1$). Second, the information about the evolved prior position $e^{\left(i\Delta\omega - \frac{\Gamma}{2}\right)dt}\xi_{k-1}$ with the evolved variance $(1-\Gamma dt)\sigma_{k-1}^2 + \sigma_{dt}^2$ is updated by an inverse-variance-weighted average with the new measured position $\left(u_m^k - O\right)$ of variance σ_n^2.

Similarly, using Eqs. (4), (7), and (10), we rewrite Eq. (8) for the probability of the next measurement as:

$$P(u_m^k | U_m^{k-1}) = \frac{1}{2\pi\sigma_n^2} e^{-\frac{\left|(u_m^k - O) - e^{\left(i\Delta\omega - \frac{\Gamma}{2}\right)dt}\xi_{k-1}\right|^2}{2\sigma_n^2}} \tag{13}$$

where we recall that $\sigma_n^2 = \frac{\eta^2\sigma^2}{\Gamma dt} \gg \sigma_{k-1}^2, \sigma_{dt}^2$ for the continuous measurement limit.

The probability density for a measurement sequence U_m^N is

$$P(U_m^N, \Delta\omega) = P(u_m^1)\prod_{k=2}^{N} P\left(u_m^k | U_m^{k-1}\right) = P(u_m^1)\prod_{k=2}^{N}\frac{1}{2\pi\sigma_n^2} e^{-\frac{\left|u_m^k - O - e^{\left(i\Delta\omega - \frac{\Gamma}{2}\right)dt}\xi_{k-1}\right|^2}{2\sigma_n^2}} \tag{14}$$

For continuous measurement, the recursive update (12) for σ_k^2 converges as $\sigma_k^2 \to \sigma_e^2 = D\eta\sigma^2$, where $D = \frac{\sqrt{\eta^2+4}-\eta}{2}$ [Supplementary Note 6: B]. With this constant variance, the continuous measurement update of the most likely position Eq. (11) becomes:

$$\xi_k = \xi_{k-1} + \left(i\Delta\omega - \tfrac{\Gamma}{2}\right)\xi_{k-1}dt + \tfrac{s\Gamma dt}{\eta}(u_m^k - O - \xi_{k-1}) \tag{15}$$

By going from the discrete to the continuous time, deriving and solving differential equations describing the time evolution of various ξ_k-dependent expectations terms in the Fisher information (Eq. (6) with (14)), the following general expression for the Fisher information can be obtained [Supplementary Note 6: C]:

$$\mathrm{I}(\Delta\omega) = I_{DRV} + I_{FL} \tag{16}$$

$$I_{DRV} = \frac{1}{\Gamma}\frac{|O|^2}{\sigma^2}\frac{4}{\left(\frac{2\Delta\omega}{\Gamma}\eta\right)^2 + \eta^2 + 4} \times \left\{\tau + \frac{1 - e^{-\Gamma\left(1+2\frac{D}{\eta}\right)\tau}}{\Gamma\left(1+2\frac{D}{\eta}\right)} - \left[\frac{e^{\left(i\Delta\omega - \frac{\Gamma}{2}\left(1+2\frac{D}{\eta}\right)\right)\tau} - 1}{i\Delta\omega - \frac{\Gamma}{2}\left(1+2\frac{D}{\eta}\right)} + c.c.\right]\right\}$$

$$I_{FL} = \frac{4}{\Gamma}\frac{D^2}{(\eta+2D)(\eta+D)} \times \left\{\tau + \frac{(\eta+D)}{D}\frac{1 - e^{-\Gamma\left(1+2\frac{D}{\eta}\right)\tau}}{\Gamma\left(1+2\frac{D}{\eta}\right)} - \frac{(\eta+2D)}{D}\frac{1 - e^{-\Gamma\left(1+\frac{D}{\eta}\right)\tau}}{\Gamma\left(1+\frac{D}{\eta}\right)}\right\}$$

and the CRLB for frequency measurement is $\mathrm{STD}(\hat{\omega}_0) \geq 1/\sqrt{\mathrm{I}(\Delta\omega)}$.

The Fisher information is the sum of two parts. The first part I_{DRV} is proportional to the modulus square of the drive-induced amplitude $|O|^2$, while the second part I_{FL} is independent of the drive and is the information contained in the stochastic fluctuations (thermodynamic and quantum-backaction induced mechanical fluctuations).

We need to emphasize the generality of the derived CRLB valid for any unbiased frequency estimator. First, the derivation made no assumptions for the relative power of white noise, described by η, meaning that it is valid for the case of any SNR. Second, it is valid for any detuning including far-detuned drive $\Delta\omega \gg \Gamma$ as long as the RWA is valid $\Delta\omega \ll \omega_0$. Third, it is valid for any averaging time τ larger than dt, including the very short averaging times, where the detection noise dominates over diffusion in the LHO position uncertainty. Finally, it is valid for any driven amplitude, including the undriven case where the eigenfrequency is extracted from fluctuations alone, i.e., I_{FL}. We also note that Eq. (16) is valid even when the stochastic force includes quantum backaction and uncertainty, as we will discuss in the next subsection. The numerical and experimental verifications of the CRLB will be discussed in the later, estimator and experimental, Sections. This result is more general than previous work[12–16], where further assumptions are made regarding measurement conditions or how the frequency is calculated from the position data, making them only valid for specific cases, such as with strong driving force or on long averaging time where the SNR is high.

This exact general formula simplifies for different useful limits as follows [Supplementary Note 6: D]:

Simplified classical CRLB for long averaging time limit. For long averaging time $\tau \gg \frac{1}{\Gamma\left(1+\frac{D}{\eta}\right)}$:

$$STD(\hat{\omega}_0) \geq \sqrt{\tfrac{\Gamma}{\tau}}\Big/\sqrt{\frac{4D^2}{(\eta+D)(\eta+2D)} + \frac{|O|^2}{\sigma^2}\frac{4}{\left[(\eta^2+4)+\left(\frac{2\Delta\omega}{\Gamma}\eta\right)^2\right]}} \tag{17}$$

where the uncertainty scales $\propto \tau^{-1/2}$, as generally expected when independent, statistically uncorrelated measurements are combined.

Simplified classical CRLB for short averaging time limit. For very short averaging $\tau \ll \frac{\eta}{\Gamma}$:

$$STD(\hat{\omega}_0) \geq 1\Big/\sqrt{\tfrac{\Gamma\tau^3}{3\eta^2}\left(\tfrac{|O|^2}{\sigma^2} + 2D^2\right)} \tag{18}$$

where the uncertainty scales $\propto \tau^{-3/2}$, as expected for a velocity measurement subject to uncorrelated position noise.

Simplified classical CRLB for weak detection noise limit. For a 'low detection noise' measurement $\eta \ll 1$, on all time scales:

$$STD(\hat{\omega}_0) \geq 1\Big/\sqrt{\tfrac{\tau}{\Gamma}\left(\tfrac{|O|^2}{\sigma^2} + 2\right)\left(1 + \eta\tfrac{1-e^{-2\frac{\Gamma}{\eta}\tau}}{2\Gamma\tau} - 2\eta\tfrac{1-e^{-\frac{\Gamma}{\eta}\tau}}{\Gamma\tau}\right)} \tag{19}$$

where, as expected, if noise is zero ($\eta = 0$), Eq. (19) recovers to the noiseless case derived independently in Supplementary Note 3 (Eqs. S10) and 4 (Eq. S16). A summary of the CRLB is presented in Supplementary Note 9.

Quantum regime

General quantum CRLB for frequency measurement. The quantum LHO subject to a continuous measurement of position is mathematically equivalent to the classical LHO with the appropriate level of measurement uncertainty and stochastic backaction force[30,31]. Therefore, the conclusions of the frequency uncertainty of classical LHO, shown in Eq. (16), can be directly extended to the quantum regime. By considering the quantum uncertainty and backaction, and using the quantum-mechanical expression for the fluctuation-dissipation theorem[33], we derive the

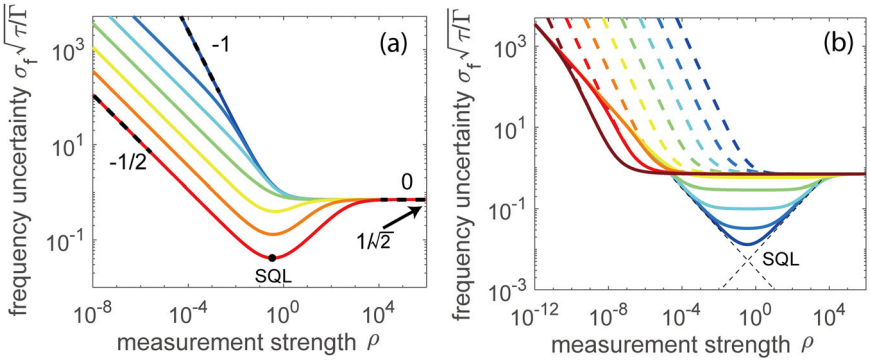

Fig. 2 Quantum limited frequency uncertainty for long measurement times. a Zero-temperature case ($T = 0$). From the blue to red lines, $\frac{|O|^2}{x^2_{ZPM}} = 0, 10^{-2}, 10^{-1}, 10^{0}, 10^{1}, 10^{2}, 10^{3}$, respectively. For a strong coherent external drive, the Standard Quantum Limit (SQL) minimum at optimal measurement strength is evident. With the weaker drive, a transition occurs, whereby the stochastic measurement backaction becomes the dominant excitation to the system, and the system's response to backaction is the dominant source of the frequency information (slope becomes -1). Dashed black lines are guides for the eye, depicting constant, linear, and square-root dependencies in the log-log plot. **b** Finite-temperature cases, with (solid lines $\frac{|O|^2}{x^2_{ZPM}} = 10^4$) and without (dashed lines $\frac{|O|^2}{x^2_{ZPM}} = 0$) external drive. From blue to red, $\frac{2k_bT}{\hbar\omega_0} = 0, 10^1, 10^2, 10^3, 10^5, 10^6, 10^7$, respectively. Increasing temperature increases the driven system uncertainty in the vicinity of the SQL, but only until the increased stochastic thermal force overtakes the drive. Larger thermal excitation at higher temperatures improves the frequency measurement in the low measurement strength regime. The detuning is set to be 0, $\frac{2\Delta\omega}{\Gamma} = 0$.

equivalent classical position uncertainty σ resulting from the temperature fluctuations and backaction. Using it together with the quantum measurement uncertainty provides the equivalent classical uncertainty ratio η. For ideal continuous quantum position measurements with zero classical detection noise and unity quantum efficiency, we obtain [See Supplementary Note 8 (Eq. S74-S76) for the derivations and the more general expressions including classical noise and non-unity quantum efficiency]:

$$\frac{\sigma^2}{x^2_{ZPM}} = \coth\frac{\hbar\omega_0}{2k_bT} + \rho \tag{20}$$

$$\eta = \frac{1}{\sqrt{2\rho\left(\coth\frac{\hbar\omega_0}{2k_bT}+\rho\right)}} \tag{21}$$

where $\rho = 4\frac{kx^2_{ZPM}}{\Gamma}$ is a dimensionless measurement strength parameter, k is the measurement strength[30], $x^2_{ZPM} = \frac{\hbar}{2m\omega_0}$ is the square of the zero-point fluctuation amplitude, $\hbar$ is the reduced Plank constant.

By applying Eqs. (20) and (21) for the parameters σ^2, η to Eqs.(16)–(19), we obtain the full quantum and thermodynamic lower limits for frequency estimation uncertainty from ideal continuous quantum position measurement.

Simplified quantum CRLB for long averaging time limit. Specifically, Eq. (17) for the long averaging time limit becomes

$$\begin{aligned} STD(\hat{\omega}_0) &\geq 1/\sqrt{I_{DRV} + I_{FL}} \\ I_{FL} &= \frac{\tau}{\Gamma}\frac{2\left(1-\frac{1}{\sqrt{1+8\rho\left(\coth\frac{\hbar\omega_0}{2k_bT}+\rho\right)}}\right)^2}{1+\frac{1}{\sqrt{1+8\rho\left(\coth\frac{\hbar\omega_0}{2k_bT}+\rho\right)}}} \\ I_{DRV} &= \frac{\tau}{\Gamma}\frac{|O|^2}{x^2_{ZPM}}\frac{1}{\coth\frac{\hbar\omega_0}{2k_bT}+\rho+\frac{1}{8\rho}\left[1+\left(\frac{2\Delta\omega}{\Gamma}\right)^2\right]} \end{aligned} \tag{22}$$

Simplified quantum CRLB for strong force noise limit. In the limit of high temperature or high measurement strength, we obtain:

$$STD(\hat{\omega}_0) \geq \sqrt{\frac{\Gamma}{\tau}}\Big/\sqrt{\frac{|O|^2}{x^2_{ZPM}\left(\coth\frac{\hbar\omega_0}{2k_bT}+\rho\right)}+2} \tag{23}$$

The standard quantum limit for frequency estimation and CRLB for quantum-backaction-driven limit. Frequency uncertainty for long averaging times [Eq. (22)] in the zero-temperature limit ($\coth\frac{\hbar\omega_0}{2k_bT} = 1$) is shown in Fig. 2(a) as a function of measurement strength for several drive strengths including zero-drive. At high drive strength (red) the term I_{DRV} dominates and we observe the typical minimum in the frequency measurement uncertainty associated with the standard quantum limit (SQL). However, with decreasing drive strength we smoothly transition to the zero external drive limit (blue) dominated by I_{FL}, in which information about the frequency is obtained from the measured system dynamics under the stochastic perturbation induced solely by the quantum measurement itself. In this zero-drive regime, the frequency measurement uncertainty linearly improves with increasing measurement strength, and then approaches a limit value $1/\sqrt{2}$ at the measurement strength $\rho \geq 1$ (the time-averaged position perturbation $\geq x^2_{ZPM}$).

In the conventional regime of drive strength larger than the measurement backaction, the frequency uncertainty monotonically increases with increasing measurement strength above the SQL. In a stark contrast, the frequency uncertainty of this new, backaction-driven measurement regime reaches a plateau at high measurement strength and does not get worse even for the measurement strength far beyond the SQL value. This backaction-dominant limit obtained at the large measurement strength, shown in Eq. (23), is independent of the stochastic force strength, provided that the stochastic fluctuations are larger than the position detection uncertainty.

Figure 2(b) shows the temperature dependence of the frequency uncertainty with and without drive. The no-drive dashed lines show the uncertainty due to the Fisher information I_{FL} obtained from the system driven stochastically by the combination of the quantum backaction and thermal fluctuations. As the mechanical fluctuation amplitude increases with higher temperatures, the uncertainty obtained for low quantum measurement strength improves.

For the driven solid lines, most of the frequency information is obtained from the response to the applied drive, I_{DRV}. The typical minimum of the uncertainty at the SQL is evident for T = 0 (blue), and deteriorates with increased temperatures due to the thermal fluctuations obscuring the driven response. However, the uncertainty increase stops at the $\mathrm{STD}(\hat{\omega}_0)\sqrt{\frac{\tau}{\Gamma}} = 1/\sqrt{2}$, explained by the additional frequency information that can be obtained from the fluctuation dynamics, I_{FL}, and that information becomes independent of the temperature and the measurement strength as shown in Eq. (23).

Maximum likelihood estimator

General frequency estimator for linear harmonic oscillators. In this section, we develop practical on-line maximum likelihood estimators for resonance frequency ω_0 from the continuously measured motion data. We demonstrate that the estimator is statistically efficient, a term used to describe estimators that reach the lowest possible uncertainty given by the CRLB.

To motivate developing an accurate frequency estimator, we note that the resonance frequency ω_0 of a resonator driven at ω is most commonly estimated by considering the steady-state response phase relative to a harmonic driving force weakly detuned from resonance: $\hat{\omega}_0 = \omega + \frac{\Gamma}{2}\left(\varphi + \frac{\pi}{2}\right)$ where $\varphi = \angle O(\Delta\omega)$ is the phase angle of $O(\Delta\omega) = \left|O(\Delta\omega)\right| e^{i\varphi}$ [14]. However, this estimator entirely neglects stochastic fluctuations, providing no frequency information when the driving force is zero. Furthermore, it is only valid for averaging times $\tau \gg \frac{1}{\Gamma}$, well above the LHO relaxation time, while for smaller τ it is biased, underestimating the frequency detuning from the drive since the motion does not have enough time to fully respond to fast frequency fluctuation. To extract the frequency at $\tau < \frac{1}{\Gamma}$ and to estimate frequency from fluctuations alone, one needs to properly consider the time derivative of the phase $d\varphi/dt$.

Here we propose a general yet computationally simple estimator that uses the full trace data U_{m}^N to obtain a frequency estimate with uncertainties reaching the CRLB limit for averaging times above and below the relaxation time $\frac{1}{\Gamma}$, for any driving force, including zero driving force, and any signal-to-noise ratio.

The frequency estimator for a measurement U_m^N returning the most likely $\Delta\omega$, satisfies $\partial P\left(U_{\mathrm{m}}^N, \Delta\omega\right)/\partial\Delta\omega = 0$, or, equivalently, $\frac{\partial}{\partial\Delta\omega}\ln P\left(U_{\mathrm{m}}^N, \Delta\omega\right) = 0$. Taking a logarithm of Eq. (14), in the continuous limit, $e^{\left(i\Delta\omega - \frac{\Gamma}{2}\right)\mathrm{d}t} \to 1$:

$$\ln P(U_{\mathrm{m}}^N, \Delta\omega) = \frac{\Gamma}{\sigma^2\eta^2}\int_0^\tau [u_{\mathrm{m}} - (\xi + O)][u_{\mathrm{m}} - (\xi + O)]^* dt \qquad (24)$$

If a good initial approximation $\Delta\omega_0$ is available for the frequency detuning $\Delta\omega$, the $\Delta\omega = \Delta\omega_0 + \delta\omega$ can be obtained by differentiating Eq. (24) and solving to the first order in $\delta\omega$ [Supplementary Note 7]:

$$\delta\omega = \frac{\int_0^\tau [(u_{\mathrm{m}}(\mathrm{t}) - (\xi + O))(\xi + O)'^* + c.c.]dt}{\int_0^\tau \left[2(\xi + O)'(\xi + O)'^* - \{(u_{\mathrm{m}}(\mathrm{t}) - (\xi + O))(\xi + O)''^* + c.c.\}\right]dt} = \frac{\hat{I}(\tau)}{\hat{J}(\tau)} \qquad (25)$$

The frequency estimate $\delta\omega$ can be obtained with low latency by real-time numerical integration of measured data u_{m}^k, to obtain the most likely position ξ and its derivatives at each time step via Eq. (15), without storing U_{m}^N in memory (Method section and Supplementary Note 7).

Simplified frequency estimator for no-detection-noise limit. Without detection noise, the general estimator can be simplified to [Supplementary Note 5]:

$$\Delta\hat{\omega} = \frac{\sum_k [(iu_k\dot{u}_k^* - i\dot{u}_k^* u_k)]}{2\sum_k u_k u_k^*} + \frac{\sum_k \left[(u_k + u_k^*)A\frac{\Gamma}{2}\right]}{2\sum_k u_k u_k^*} \qquad (26)$$

with $\dot{u}_k$ defined as $\dot{u}_k = \left(u_{k+1} - u_k\right)/\mathrm{d}t$. The first term shows the frequency information contained in the phase gradient, while the second term stands for the conventional phase part. This noiseless form generalizes the commonly used phase[14] and phase gradient[27] estimators.

Numerical verification. To numerically verify the derived CRLB and the estimator we apply them to simulated LHO motion data u_k obtained using Eq. (2) with the LHO parameters from our experimental system with $\omega_0/2\pi \approx 27.8$ MHz, $\Gamma/2\pi \approx 620$ Hz (Q ≈ 44800), $m \approx 1$ pg, and $T \approx 293$ K. The random Langevin forces $f_{1,2}$ are picked from a zero-mean Gaussian with the variance $\mathrm{Var}(f_1) = \mathrm{Var}(f_2) = \frac{\Gamma k_b T m}{\mathrm{d}t}$ [19,34]. We add artificial Gaussian detection noise to the simulated u_k, and extract the frequency $\Delta\omega_{n\tau}$ from the processed data set $U_{\mathrm{m}}^{N,n}$ using Eq. (25) [see Method section and Supplementary Note 7 for the detail of the algorithm].

We compare the CRLB from Eq. (16) to the Allan variance of the frequency estimates $\Delta\omega_{n\tau}$ generated from a series of simulated motion segments $U_{\mathrm{m}}^{N,n}$, each of length τ. The Allan variance is calculated as a weighted average:

$$\sigma_f^2(\tau) = \frac{1}{2}\left\langle W_{n\tau}[\Delta\omega_{(n+1)\tau}/2\pi - \Delta\omega_{n\tau}/2\pi]^2\right\rangle_{T_0} \qquad (27)$$

where $\langle\ldots\rangle_{T_0}$ represents the average of the data over the total time T_0 for all segments and $W_{n\tau}$ represents the weight of each element. The inverse-variances-weights $W_{n\tau} = \left(\hat{J}_n/\langle\hat{J}_n\rangle_{T_0}\right)^2$ account for the changes in the variance between the frequency estimates for $\tau < 1/\Gamma$. The weights converge to $W_{n\tau} \approx 1$ as in the conventional Allan variance [28] when averaging time is long $\tau \gg 1/\Gamma$, or the drive is strong $O(\Delta\omega) \gg \sigma$.[Supplementary Note 5 or 7 for the case with or without detection noise]

Figure 3(a) shows the Allan deviation (ADEV) of the estimated frequency from the numerically simulated data with artificial Gaussian detection noise of $\eta = 0.1$. Both undriven and driven cases present a good agreement to the CRLB given by Eq. (16). Besides the good agreement, one would also notice that at $\tau \ll \frac{\eta}{\Gamma}$, ADEV and CRLB are $\propto \tau^{-3/2}$ as predicted by Eq. (18), while at $\tau \gg \frac{\eta}{\Gamma}$, ADEV and CRLB are $\propto \tau^{-1/2}$ as in Eq. (17). We show the driven case of different detuning of 0, Γ and 10Γ in Fig. 3(b). The uncertainty of the estimated frequency increases with the detuning as the steady-state LHO amplitude becomes lower. The proposed estimator and the CRLB work for any detuning within the RWA validity.

Figure 3(c), (d) show the undriven and driven cases with different detection noise $\eta = 0.01, 0.1, 1, 10$. For the driven case Fig. 3(d), the detection noise negligibly affects the ADEV at long time scale, evident by the good agreement between ADEV and the noiseless CRLB (dashed line) at $\tau \gg \frac{\eta}{\Gamma}$. However, for the undriven case Fig. 3(c), when $\eta > 1$, the detection noise not only affects the short time scale frequency estimation but also degrades precision at the long time scale ($\tau \gg \frac{\eta}{\Gamma}$), where the detection noise becomes comparable to the fluctuating mechanical motion signal.

Overall, the proposed computationally simple and general frequency estimator works over broad time scales, any driving force, detuning, and detection noise levels. Importantly, it can be directly applied to low signal-to-noise-ratio data, which makes it work well for very high-bandwidth measurements. In comparison, the conventional phase estimator fails when the driving force is weak or for short averaging times, and the phase-gradient

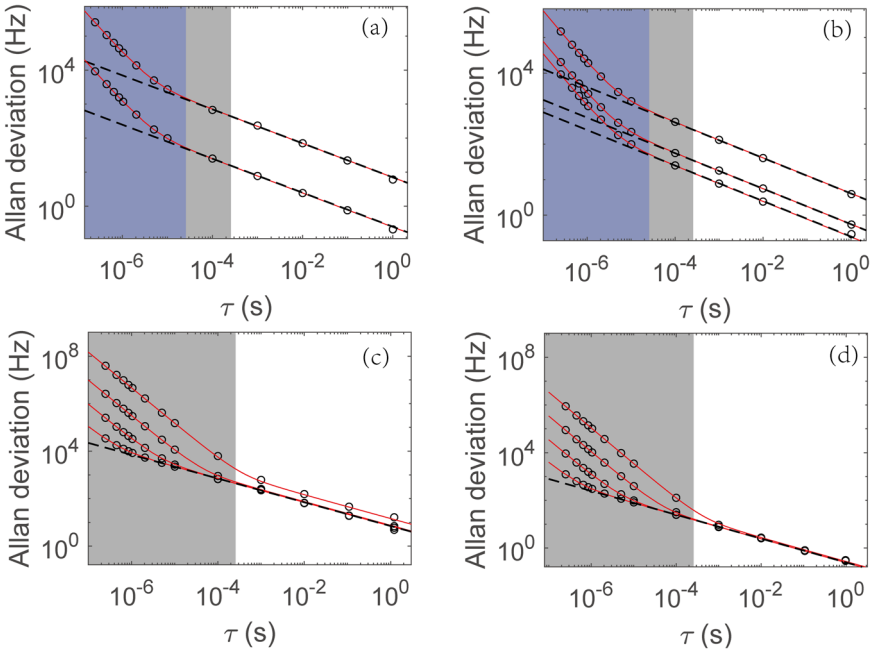

Fig. 3 Frequency Allan deviation and Cramer Rao lower bound for simulated data with added Gaussian detection noise. a Undriven (A = 0, top line) and driven cases (A = 40σ, bottom line) with $\eta = 0.1$ and $\Delta\omega = 0$. Black circles are Allan deviation (ADEV) of the frequency estimated by Eq. (25), red solid lines are the corresponding Cramer Rao lower bound (CRLB), Eq. (16), black dashed lines are noiseless CRLB Eq. (19) with $\eta = 0$. The blue and gray shades label $\tau < \frac{\eta}{\Gamma}$ and $\tau < \frac{1}{\Gamma}$, respectively. **b** Driven case (A = 40σ) with detuning $\Delta\omega = 0$, Γ, and 10Γ (from bottom to top), and $\eta = 0.1$. **c**, **d** Undriven (A = 0) and driven (A = 40σ) cases, respectively, with varying added noise level $\eta = 0.01$, 0.1, 1, 10 (from bottom to top) and constant $\Delta\omega = 0$. The one standard deviation uncertainties of the data points obtained from the numerical simulation are smaller than the symbol size.

estimator fails at all time scales when the detection noise is non-negligible. The maximum likelihood estimator reaches the CRLB limit which shows the estimator is statistically efficient, i.e., extracting the maximum degree of frequency information and producing the lowest possible uncertainty. The numerical validation indicates that both the frequency estimator and the CRLB are valid. We further verify them experimentally.

Experimental verification. As shown in Fig. 1(a), the resonance frequency of the nanoscale tuning fork ($\omega_0/2\pi \approx 27.8$ MHz) is estimated from its mechanical displacement signal produced by a cavity-optomechanical readout (see Supplementary Note 1)[35]. Figure 4(a) shows the statistical distributions in the phase-diagram of the time-domain mechanical displacement of the tuning fork under driving forces of different magnitude, indicating Gaussian profiles with similar variance $\sigma^2 \approx 2.3 \times 10^{-8}\,\mathrm{V}^2$. Figure 4(b) shows the power spectral density of the tuning fork driven by only the Langevin force. The Lorentzian fit and energy autocorrelation analysis show $\Gamma/2\pi \approx 620$ Hz [see Supplementary Note 1]. The detection noise ratio $\eta \approx 0.08$ is independently estimated from the position noise power spectral density spectra.

Four groups of data are analyzed for independently extracted $A = 0$, 5.1σ, 10.4σ, 16.5σ, shown in Fig. 4(c), corresponding to the four groups of data shown in Fig. 4(a). The data shows similar features to Fig. 3(a), and good agreement with the CRLB is observed over three to four decades of averaging time, without adjustable parameters. At small τ, the frequency stability tends toward $\tau^{-3/2}$ due to detection noise. The frequency uncertainty reaches the thermodynamic limit for these drive strengths at $\tau \approx 0.1\,\mathrm{ms} < 1/\Gamma$ and remains at this limit for up to $\tau \approx 0.5$ s.

Notably, the relative frequency bias stability of the undriven stress-engineered resonator (light blue line) is measured to be lower than 0.4×10^{-6} for up to ≈1 s averaging. This is better than the average performance of the state-of-the-art strongly driven NEMS in such mass range (≈ 1 pg)[15], demonstrating that continuous passive frequency measurement from thermal fluctuations is a viable practical approach for high-performance frequency-based sensing. Using thermal fluctuations simplifies the device by eliminating the actuator and simplifies the detection apparatus by removing the need to apply an electrical or optical drive signal. Naturally present white Langevin force substitutes for the often-used frequency tracking feedback circuitry needed to keep the drive frequency on resonance. Multiple, separately detected mechanical resonators can be used, e.g. for differential measurements, without the risk of errors and frequency locking due to drive signal crosstalk. The frequency estimator we have developed makes the real-time continuous measurement of frequency from thermal fluctuations practical. In one example, multiple unpowered frequency-based NEMS sensors connected by an optical fiber cable can be remotely interrogated with a single tuneable low-power continuous-wave laser, without the need for electrical connections of any kind.

With increasing driving force, the CRLB of frequency goes down. Impressively, the experimental measurement of the frequency of the strongly driven resonator (purple line) illustrates that very fast changes in the resonance frequency on the time scales 30–100 μs ($\ll 1/\Gamma$) can be continuously tracked with only a few parts per million (ppm) uncertainty on average – opening up yet another high performance sensing regime for practical applications. Importantly, it is clearly experimentally observed that the $\tau^{-1/2}$ scaling continues well below 1/Γ [about 1/(3Γ) here], before being taken over by the instrumental noise contribution scaling as $\tau^{-3/2}$. This agrees with our theoretical analysis, and firmly establishes the thermodynamic limit for $\tau < 1/\Gamma$. It also practically shows that frequency changes can be sensed with low noise on short time scales not limited by the resonator relaxation time. In fact, longer relaxation times (lower Γ) will lead to lower frequency uncertainty

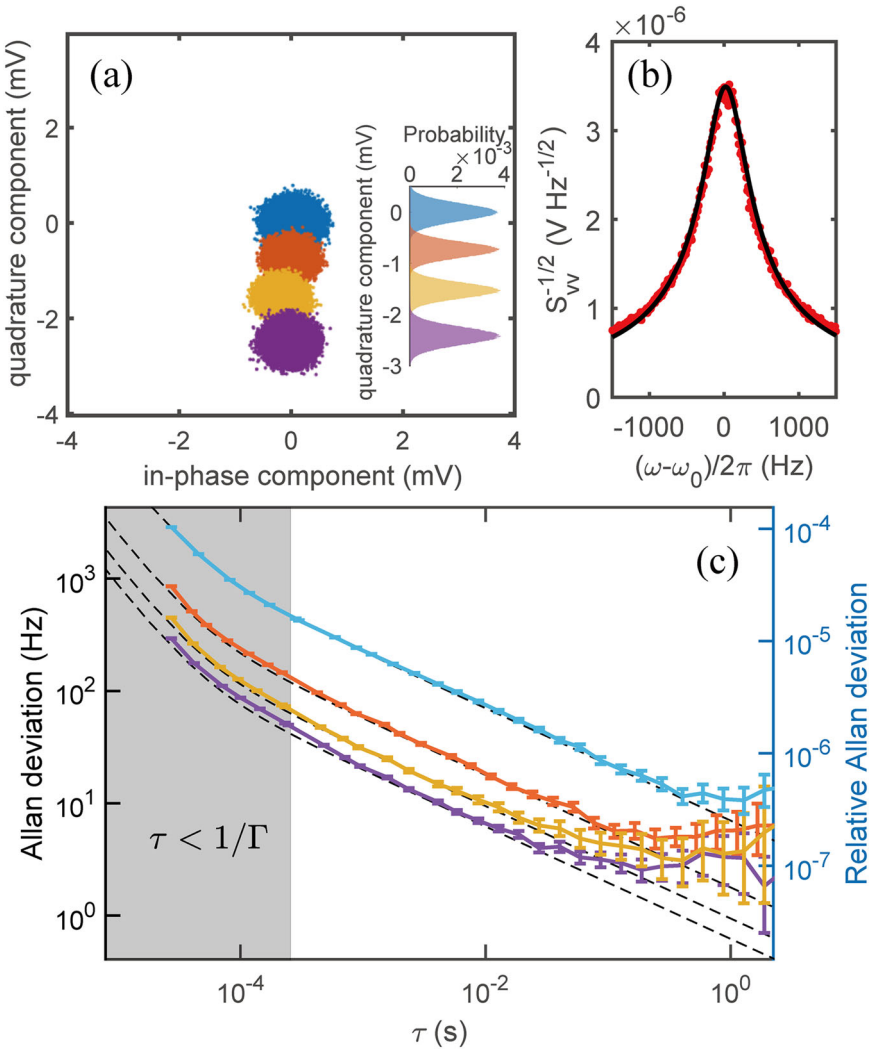

Fig. 4 Experimental data. a Thermal fluctuation of the nanomechanical resonator in the phase diagram. Different colors correspond to different driving forces (0 V, 0.5 V, 1 V, and 1.5 V). The driving/reference frequency is set near the resonance frequency. The inset shows the distribution density of the quadrature component. **b** Mechanical vibration power spectral density in vacuum. The black line indicates the Lorentzian fit. **c** Allan deviation (ADEV) of the frequency from the experimental data without drive (light blue) and with increasing driving forces (from top to bottom). The ADEVs are from the data sets of the corresponding colors in (**a**). Dashed lines are the corresponding Cramer Rao lower bound. The deviation at $\tau > 0.1$ s is due to bias drift. The marked experimental statistical uncertainties are one standard deviation.

for the given linear drive, provided the detection is sufficiently low noise. Our analysis quantitatively defines the measurement bandwidth over which the measurement is thermodynamically, rather than detection-noise, limited, and shows how this bandwidth increases with decreasing detection noise.

The frequency uncertainty deviates from the thermodynamic limit at long averaging times. For τ longer than ≈ 1.18 s, 0.24 s, 0.26 s, and 0.19 s, from undriven to strongly driven cases, the ADEVs reach the relative bias stability of $(0.363 \pm 0.062) \times 10^{-6}$, $(0.194 \pm 0.018) \times 10^{-6}$, $(0.133 \pm 0.038) \times 10^{-6}$, and $(0.108 \pm 0.012) \times 10^{-6}$. The relative bias stability improves with increasing drive strength. We attribute the observed slow bias drift to slow changes in temperature, mechanical stress, or electrostatic charging in the device.

Discussion

We have derived the Cramer Rao Lower Bound on the uncertainty of the resonance frequency measurement under a wide, general range of measurement conditions. The CRLB defines fundamental quantum and thermodynamic limits of the best possible frequency estimation from a continuous position measurement [see Supplementary Note 9 for a summary of CRLB in different conditions]. Mathematically, the measured trajectory contains two distinct and independent contributions to the Fisher information about frequency–the first coming from the system's response to the applied harmonic drive and the second coming from the response to the stochastic forces: the Langevin force and the quantum measurement backaction. The information-theoretic approach for deriving the fundamental measurement limits is general and explicit, avoiding any hidden assumptions about the system physics, making our results exact for any system described by the linear harmonic oscillator model, either classical or quantum.

The theoretical frequency uncertainty limits are only reached practically if the frequency is calculated from the recorded position trajectory by a statistically efficient estimator procedure, i.e., a procedure that uses all available information without information loss. We derive a maximum-likelihood estimator for eigenfrequencies that seamlessly includes Fisher information from the system response to both the driving and stochastic forces, and verify it on simulated position data. For all time scales

considered, including very short time scales, the estimated eigenfrequency agrees with the simulation-specified value and the Allan deviation achieves the CRLB limit, showing the estimator is unbiased and statistically efficient. Importantly, the estimator can be used for data with any degree of detection noise, and its noiseless form unifies the commonly used phase and phase gradient estimators. The estimator can be applied to any physical system that can be validly described as a linear harmonic oscillator with continuously measured position, including both classical and quantum LHO.

In this work, we assume both the position noise (quantum and classical) and the force noise (backaction and thermal) are uncorrelated white noises at least over the frequency window given by the highest measurement bandwidth and centered on the resonance. This assumption is often valid, particularly for the narrow measurement bandwidths used in resonance-based metrology of high-quality factor oscillators. For broad bandwidth measurements of oscillators subject to correlated noise sources, one can rederive the frequency detection limit and the estimator for the specific form of correlated noises using the method proposed in this work, although there may not be a simple analytical expression anymore.

We use the estimator to experimentally measure the resonance frequency of a high-quality-factor nanomechanical resonator with an integrated cavity-optomechanical readout, and demonstrate that, quantitatively and without adjustable parameters, the frequency uncertainty reaches the predicted CRLB thermodynamic limits over a broad range of integration times and drive strengths. The nanomechanical resonator shows low frequency uncertainty in the undriven/weakly driven regime and at very high measurement bandwidths (short averaging times). Beyond the field of nanomechanical sensing and transduction, the presented theoretical and experimental results are broadly applicable to mechanical, optical, acoustic, radiofrequency, and other linear oscillator systems. This work advances the general understanding of harmonic oscillator frequency measurement by generalizing and extending the better-understood and commonly used regime of strong drive and long averaging time to, first, the regime of weak or no drive and, second, of very short averaging times. It firmly establishes opportunities and provides theoretical limits for very high bandwidth sensing and for fluctuation-based frequency sensing without external power, such as frequency-sensing solely using quantum measurement backaction. It provides a universal prescription for extracting harmonic oscillator frequency from its continuously measured position that is both practical and achieving fundamental limits of precision. Finally, this work combines a rigorous description and a simple, intuitive interpretation of the quantum limits covering all these regimes.

Methods

Maximum likelihood estimator Eq. (25) via direct numerical integration. Here we summarize a computationally efficient on-line integration procedure for estimating $\delta\omega$. Note, we have $O = \frac{iA_{\frac{\Gamma}{2}}^{\Gamma}}{i\Delta\omega - \frac{\Gamma}{2}}$, $O' = \frac{A_{\frac{\Gamma}{2}}^{\Gamma}}{\left(i\Delta\omega - \frac{\Gamma}{2}\right)^2}$, $O'' = -\frac{iA\Gamma}{\left(i\Delta\omega - \frac{\Gamma}{2}\right)^3}$ and a known $\Delta\omega$ with $\delta\omega(0) = 0$. In the continuous detection limit where $s = s_e = D$, we have the following from Eq. (15) and its first- and second-order derivative on $\Delta\omega$:

$$d(\xi + O) = \left(i\Delta\omega - \tfrac{\Gamma}{2}\right)((\xi + O) - O)dt + \tfrac{D}{\eta}\Gamma(u_{\mathrm{m}} - (\xi + O))dt \tag{28}$$

$$d(\xi + O)' = i((\xi + O) - O)dt + \left(i\Delta\omega - \tfrac{\Gamma}{2}\right)\left((\xi + O)' - O'\right)dt - \tfrac{D}{\eta}\Gamma(\xi + O)'dt \tag{29}$$

$$d(\xi + O)'' = 2i((\xi + O)' - O')dt + \left(i\Delta\omega - \tfrac{\Gamma}{2}\right)((\xi + O)'' - O'')dt - \tfrac{D}{\eta}\Gamma(\xi + O)'' \tag{30}$$

Going back to the discrete-time and defining variables:

$$\begin{cases} \alpha_k = (\xi + O)_k \\ \beta_k = (\xi + O)'_k \\ \gamma_k = (\xi + O)''_k \end{cases} \tag{31}$$

we start with $\alpha_0 = \alpha_{N,\,previous}$ where $\alpha_{N,\,previous}$ is from the previous segment of data, $\beta_0 = \gamma_0 = 0$. Initial detuning $\Delta\omega_0$ needs to be provided with $\delta\omega(0) = 0$. Then we begin finite difference time domain integration.

From Eq. (28), we have:

$$\alpha_k - \alpha_{k-1} = \left(i\Delta\omega_0 - \tfrac{\Gamma}{2}\right)\left[\tfrac{(\alpha_k + \alpha_{k-1})}{2} - O\right]dt + \tfrac{D}{\eta}\Gamma\left[u_{\mathrm{m}}^k - \tfrac{(\alpha_k + \alpha_{k-1})}{2}\right]dt \tag{32}$$

Note, we use the averaged value of two adjacent points to do the integration for numerical accuracy.

Similarly, from Eqs. (29) and (30) we have:

$$\beta_k - \beta_{k-1} = i(\alpha_{k-1} - O)dt + \left(i\Delta\omega_0 - \tfrac{\Gamma}{2}\right)\left[\tfrac{(\beta_k + \beta_{k-1})}{2} - O'\right]dt - \tfrac{D}{\eta}\Gamma\tfrac{(\beta_k + \beta_{k-1})}{2}dt \tag{33}$$

$$\gamma_k - \gamma_{k-1} = 2i(\beta_k - O')dt + \left(i\Delta\omega_0 - \frac{\Gamma}{2}\right)\left[\frac{(\gamma_k + \gamma_{k-1})}{2} - O''\right]dt - \frac{D}{\eta}\Gamma\frac{(\gamma_k + \gamma_{k-1})}{2}dt \tag{34}$$

Defining two more variables following updates:

$$I_k = I_{k-1} + \left[\left(u_{\mathrm{m}}^k - \tfrac{(\alpha_k + \alpha_{k-1})}{2}\right)\beta_k^* + c.c.\right]dt \tag{35}$$

$$J_k = J_{k-1} + \left[2\beta_k\beta_k^* - \left\{\left(u_{\mathrm{m}}^k - \tfrac{(\alpha_k + \alpha_{k-1})}{2}\right)\tfrac{(\gamma_k + \gamma_{k-1})}{2}^* + c.c.\right\}\right]dt \tag{36}$$

with initial conditions $I_0 = J_0 = 0$.

After doing N iterations during measurement time $\tau = Ndt$, based on Eq. (25) we obtain the frequency estimated as:

$$\delta\omega_\tau = \frac{I_N}{J_N} \tag{37}$$

The measured frequency during this measurement time interval is then

$$\Delta\omega_\tau = \Delta\omega_0 + \delta\omega_\tau = \Delta\omega_0 + \frac{I_N}{J_N}$$

We can then continue to the next measurement by setting

$$\alpha_0 \leftarrow \alpha_N$$

and resetting $\beta_0 = \gamma_0 = I_0 = J_0 = 0$ and $\delta\omega_\tau = 0$.

Data availability

The data that support the plots within this paper are available from the corresponding author upon a reasonable request.

Code availability

The code that supports the theoretical plots within this paper is available from the corresponding author upon a reasonable request.

Received: 17 March 2021; Accepted: 30 July 2021;
Published online: 15 September 2021

References

1. LIGO Scientific and Virgo Collaboration. et al. GW170104: observation of a 50-solar-mass binary black hole coalescence at redshift 0.2. *Phys. Rev. Lett.* **118**, 221101 (2017).
2. Chaste, J. et al. A nanomechanical mass sensor with yoctogram resolution. *Nat. Nanotech* **7**, 301–304 (2012).
3. Losby, J. E. et al. Torque-mixing magnetic resonance spectroscopy. *Science* **350**, 798–801 (2015).
4. Cleland, A. N. & Roukes, M. L. A nanometre-scale mechanical electrometer. *Nature* **392**, 160–162 (1998).
5. Sauer, V. T. K., Diao, Z., Westwood-Bachman, J. N., Freeman, M. R. & Hiebert, W. K. Single laser modulated drive and detection of a nano-optomechanical cantilever. *AIP Adv.* **7**, 015115 (2017).
6. Barnard, A. W., Zhang, M., Wiederhecker, G. S., Lipson, M. & McEuen, P. L. Real-time vibrations of a carbon nanotube. *Nature* **566**, 89–93 (2019).
7. Rugar, D., Budakian, R., Mamin, H. J. & Chui, B. W. Single spin detection by magnetic resonance force microscopy. *Nature* **430**, 329–332 (2004).
8. Naik, A. K., Hanay, M. S., Hiebert, W. K., Feng, X. L. & Roukes, M. L. Towards single-molecule nanomechanical mass spectrometry. *Nat. Nanotech* **4**, 445–450 (2009).
9. Tanaka, M. An industrial and applied review of new MEMS devices features. *Microelectron. Eng.* **84**, 1341–1344 (2007).

10. Giessibl, F. J. & Bielefeldt, H. Physical interpretation of frequency-modulation atomic force microscopy. *Phys. Rev. B* **61**, 9968–9971 (2000).
11. Albrecht, T. R., Grütter, P., Horne, D. & Rugar, D. Frequency modulation detection using high-Q cantilevers for enhanced force microscope sensitivity. *J. Appl. Phys.* **69**, 668–673 (1991).
12. Cleland, A. N. & Roukes, M. L. Noise processes in nanomechanical resonators. *J. Appl. Phys.* **92**, 2758–2769 (2002).
13. Ekinci, K. L., Yang, Y. T. & Roukes, M. L. Ultimate limits to inertial mass sensing based upon nanoelectromechanical systems. *J. Appl. Phys.* **95**, 2682–2689 (2004).
14. Gavartin, E., Verlot, P. & Kippenberg, T. J. Stabilization of a linear nanomechanical oscillator to its thermodynamic limit. *Nat. Commun.* **4**, 2860 (2013).
15. Sansa, M. et al. Frequency fluctuations in silicon nanoresonators. *Nat. Nanotech* **11**, 552–558 (2016).
16. Roy, S. K., Sauer, V. T. K., Westwood-Bachman, J. N., Venkatasubramanian, A. & Hiebert, W. K. Improving mechanical sensor performance through larger damping. *Science* **360**, eaar5220 (2018).
17. Campos, A. D. An extension of the Cramér-Rao inequality for the sequential case. *Trabajos de. Estad. y. de. Investigacion Operativa* **30**, 65–70 (1979).
18. Malécot, G. Statistical methods and the subjective basis of scientific knowledge. *Genet. Selection Evolution* **31**, 269 (1999).
19. Gardiner, C. W. *Handbook of stochastic methods.* Vol. 3 (Springer Berlin, 1985).
20. Rissanen, J. J. Fisher information and stochastic complexity. *IEEE Trans. Inf. Theory* **42**, 40–47 (1996).
21. Errico, C. et al. Ultrafast ultrasound localization microscopy for deep super-resolution vascular imaging. *Nature* **527**, 499–502 (2015).
22. Zhou, Y., Handley, M., Carles, G. & Harvey, A. R. Advances in 3D single particle localization microscopy. *APL Photonics* **4**, 060901 (2019).
23. Parthasarathy, R. Rapid, accurate particle tracking by calculation of radial symmetry centers. *Nat. Methods* **9**, 724–726 (2012).
24. Smith, C. S., Joseph, N., Rieger, B. & Lidke, K. A. Fast, single-molecule localization that achieves theoretically minimum uncertainty. *Nat. Methods* **7**, 373–375 (2010).
25. Berni, A. A. et al. Ab initio quantum-enhanced optical phase estimation using real-time feedback control. *Nat. Photonics* **9**, 577–581 (2015).
26. Lee, S.-Y., Lee, C.-W., Lee, J. & Nha, H. Quantum phase estimation using path-symmetric entangled states. *Sci. Rep.* **6**, 30306 (2016).
27. Kay, S. A fast and accurate single frequency estimator. *IEEE Trans. Acoust., Speech, Signal Process.* **37**, 1987–1990 (1989).
28. Allan, D. W. Time and Frequency (Time-Domain) Characterization, Estimation, and Prediction of Precision Clocks and Oscillators. *IEEE Trans. Ultrason., Ferroelect., Freq. Contr.* **34**, 647–654 (1987).
29. Liu, Y., Miao, H., Aksyuk, V. & Srinivasan, K. Wide cantilever stiffness range cavity optomechanical sensors for atomic force microscopy. *Opt. Express, OE* **20**, 18268–18280 (2012).
30. Jacobs, K. *Quantum Measurement Theory and its Applications.* (Cambridge University Press, 2014).
31. Clerk, A. A., Devoret, M. H., Girvin, S. M., Marquardt, F. & Schoelkopf, R. J. Introduction to quantum noise, measurement, and amplification. *Rev. Mod. Phys.* **82**, 1155–1208 (2010).
32. Gelman, A. *Bayesian data analysis.* (CRC Press, 2014).
33. Hänggi, P. & Ingold, G.-L. Fundamental aspects of quantum Brownian motion. *Chaos* **15**, 026105 (2005).
34. Landau, L. D. & Lifshitz, E. M. *Statistical Physics.* Vol. 5 (Course of theoretical physics 3, 1994).
35. Wang, M., Zhang, R., Ilic, R., Aksyuk, V. & Liu, Y. Frequency Stabilization of Nanomechanical Resonators Using Thermally Invariant Strain Engineering. *Nano Lett.* **20**, 3050–3057 (2020).

Acknowledgements

We thank Dr. Michael Zwolak, Dr. Daniel Lopez, Dr. Linhai Huang, Dr. Christopher Wallin, Dr. J. Alexander Liddle and Dr. Marcelo Davanco for reviewing this paper and giving meaningful suggestions. M.W. is supported by the Cooperative Research Agreement between the University of Maryland and the National Institute of Standards and Technology Center for Nanoscale Science and Technology, Award 70NANB10H193, through the University of Maryland;

Author contributions

V.A. conceived and designed the research. M.W. and V.A. conduct the theoretical derivation and simulation; R.Z., R.I. and Y.L developed the fabrication process and fabricated the devices. R.Z. and Y.L. conducted the experiment. M.W. and V.A. analyzed the experimental data.

Competing interests

The authors declare no competing interests.

Additional information

Supplementary information The online version contains supplementary material available at https://doi.org/10.1038/s42005-021-00700-6.

Correspondence and requests for materials should be addressed to Vladimir A. Aksyuk.

Peer review information *Communications Physics* thanks Raimundo Costa Filho and Fabio Grazioso for their contribution to the peer review of this work. Peer reviewer reports are available.

Reprints and permission information is available at http://www.nature.com/reprints

Publisher's note Springer Nature remains neutral with regard to jurisdictional claims in published maps and institutional affiliations.